Wave extremes diverge from mean conditions under climate change

Héctor Lobeto[1], Gil Lemos[2], Mercè Casas-Prat[3], Mark Hemer[4], Alberto Meucci[5], Nobuhito Mori[6], Rajesh Kumar[7], Alvaro Semedo[8], Leah Cicon[3], Benoit Pouliot[3], Melisa Menendez[1], Iñigo J. Losada[1], Mikhail Dobrynin[9], Remya P G[10], Mithun Sundhar B[10], Tomoya Shimura[6], Stephane Law Chune[11], Meenakshi Sreejith[11], Lucy Bricheno[12], Ben Timmermans[12], Claire Trenham[4], Ian R. Young[5], David Gutierrez[13], Borja Reguero[13], Sofia Caires[14]

[1] IHCantabria - Instituto de Hidráulica Ambiental de la Universidad de Cantabria
[2] Instituto Dom Luiz (IDL), Faculdade de Ciências, Universidade de Lisboa, Campo Grande, 1749–016, Lisboa, Portugal
[3] Environment and Climate Change Canada, Climate Research Division
[4] CSIRO Environment, Australia
[5] Department of Infrastructure Engineering, The University of Melbourne
[6] Disaster Prevention Research Institute, Kyoto University
[7] Centre for Climate Research Singapore, Meteorological Service Singapore, 537054, Singapore
[8] Department of Coastal and Urban Risk and Resilience, IHE Delft Institute for Water Education, Delft, The Netherlands.
[9] Deutscher Wetterdienst (DWD), Hamburg, Offenbach am Main, Germany
[10] Indian National Centre for Ocean Information Services (INCOIS), MoES, Hyderabad, India
[11] Mercator Ocean International, Toulouse, France
[12] National Oceanography Centre, European Way, Southampton, SO14 3ZH, UK
[13] Center for Coastal Climate Resilience, University of California, Santa Cruz, CA, 95060, USA
[14] Deltares, Delft, The Netherlands

Bias Assessment

Climate model simulations aim to represent the intrinsic behavior of the real climate system, capturing the complex interactions between the atmosphere, the ocean, the land surface, and sea ice (REF WG1 AR6). As a result of this complexity, the model-based simulations (in which the COWCliP-3 ensemble is included) may exhibit systematic biases relative to reference or observed conditions68. Assessing these biases is therefore a fundamental step to establish the level of evidence supporting the interpretation of projected changes in wave climate as represented by COWCLiP-3.

The ensemble shows good performance when evaluated against reference reanalysis and satellite altimetry observations (Figure 1 and Figure SM1, respectively). Biases in mean significant wave height (H_s) are modest across most of the global ocean, with consistent spatial patterns relative to both reference datasets. A widespread overestimation of mean H_s (Figure 1a) and 95th percentile Hs (Figure 1b) is present, except in a few tropical regions, the far northern Atlantic and the Mediterranean Sea. Additionally, relatively large biases are present in narrow straits and small island regions, related to differences in native horizontal resolution between ensemble members. Maximum biases occur in Southern Hemisphere (SH) mid-latitudes, ranging between +10% and +20%; overestimations in the North Pacific mid-latitudes are of similar magnitude, and exceed 20% in northeast tropical Pacific and the Bay of Bengal. Biases in mean direction (Dir_m) and peak period (T_p) also remain limited globally (Figure SM2).

Variability is generally well reproduced. Biases in intra-annual variability (Figure 1c) remain below 5% across most of the global ocean, yet overestimations dominate. Interannual variability (Figure 1d) exhibits similar patterns: systematic overestimations, generally below 5%, except at very high latitudes, where sea-ice interaction plays a key role in wave generation.

Overall, the ensemble reproduces historical wave conditions with reasonable accuracy across most oceanic regions, providing an adequate basis for assessing projected changes. It should be noted that while ensemble members with low biases are generally considered more reliable, historical performance does not necessarily correlate with ability to reproduce the climate change signal. Nevertheless, as the analysis focuses on relative changes, systematic biases are not expected to substantially affect the spatial patterns and signs of projected responses.

Tables

Institution	Model	Scenario			Period		Model	Variables			
		SSP1-2.6	SSP2-4.5	SSP5-8.5	Mid	End		Hs	Tp	CgE	Dirm
CCRS	EC-Earth3	■		■	■	■	WW3	■	■	■	■
	ACCESS-CM2	■		■	■	■	WW3	■	■	■	■
	CMCC-CM2-SR5	■		■		■	WW3	■	■	■	■
	IPSL-CM6A-LR	■		■	■	■	WW3	■	■	■	■
	HadGEM3-GC31-MM	■		■		■	WW3	■	■	■	■
	CNRM-CM6-1-HR	■		■		■	WW3	■	■	■	■
	MPI-ESM1-2-HR	■		■	■	■	WW3	■	■	■	■
	MIROC6	■		■		■	WW3	■	■	■	■
ECCC	CanESM5		■	■	■	■	WW3	■	■		■
IHC	EC-Earth3		■	■	■	■	WW3	■	■	■	■
	MRI-ESM2-0		■	■	■	■	WW3	■	■	■	■
	CNRM-CM6-1-HR		■	■	■	■	WW3	■	■	■	■
	MPI-ESM1-2-HR		■	■	■	■	WW3	■	■	■	■
IDL	EC-Earth3			■		■	WW3	■	■	■	■
	EC-Earth3			■		■	WW3	■	■	■	■
	EC-Earth3			■		■	WAM	■	■	■	■
INCOIS	MPI-ESM1-2-HR		■	■	■	■	WW3	■	■	■	■
	BCC-CSM2-MR		■	■	■	■	WW3	■	■	■	■
MOI	CNRM-CM6-1-HR	■		■	■	■	WAM	■	■		■
NOC	HadGEM3-GC31-MM	■		■	■	■	WW3	■	■		■
	CNRM-CM6-1-HR	■			■	■	WW3	■	■		■
	GFDL-CM4	■			■	■	WW3	■	■		■
CSIRO-UoM	EC-Earth3	■		■	■	■	WW3	■	■	■	■
	ACCESS-CM2	■		■	■	■	WW3	■	■	■	■
	AWI-CM1-1-MR	■		■		■	WW3	■	■	■	■
	CMCC-CM2-SR5	■		■		■	WW3	■	■	■	■
	IPSL-CM6A-LR	■		■		■	WW3	■	■	■	■
	KIOST-ESM	■		■		■	WW3	■	■	■	■
	MRI-ESM2-0	■		■		■	WW3	■	■	■	■
	MPI-ESM1-2-LR	■		■		■	WW3	■	■	■	■

Table SM1: Description of the ensemble members. The generating institution, the forcing GCM, the scenarios covered, the projection horizon periods considered, the wave propagation model used, and the variables provided are specified. The gray shading indicates whether that element is present for a given ensemble member. WW3 is the abbreviation for WaveWatchIII.

Scenario	Horizon period	Variable							
		Mean H_s	P95 H_s	Mean T_p	P95 T_p	Mean C_gE	Mean Dir_m	TH ext H_s	LF ext H_s
Historical		30	30	30	30	25	30	26	27
SSP1–2.6	Mid-century	10	10	10	10	6	10	10	10
	End-Century	20	20	20	20	16	20	20	20
SSP2–4.5	Mid-century	7	7	7	7	6	7	6	6
	End-Century	7	7	7	7	6	7	6	6

SSP5–8.5	Mid-century	15	15	15	15	12	15	14	14
	End-Century	28	28	28	28	25	28	26	27

Table SM2: Distribution of ensemble members across periods and scenarios. Number of available members for each combination of time horizon, scenario, variable, and metric considered. TH refers to threshold exceedances and LF to low frequency.

Institution	Wave model	Version	Global resolution	Source term	Ice param.
CCRS	WaveWatch III	V7.12	0.0088 deg (lon) x 0.0056 deg (lat)	ST4	IC0
ECCC	WaveWatch III	V7.00	0.36 deg	ST4	IC0/IS0
IHC	WaveWatchIII	v7.00	0.5 deg	ST4	IC2/IS2
IDL	WaveWatch III (2) / WAM (1)	V6.07 (2) / v4.6 (1)	0.7 deg	ST4, ST6 / Cy45R1 (~ST3)	IC0 (2) / FLT (1)
INCOIS	WaveWatch III	V6.07	0.5 deg	ST4	IC0
MOI	WAM	MF-WAMcy42	1.0 deg	ST4	Yu et al. 2021
NOC	WaveWatch III	v7.00	0.5 deg	ST4	IC0/IS0
CSIRO-UoM	WaveWatch III	V6.07	0.5 deg	ST6	IC0

Table SM3: Numerical configuration of the climate simulations. Table includes: developing institution, numerical model, numerical model version, global spatial resolution, source term, and ice parameterization.

Figures

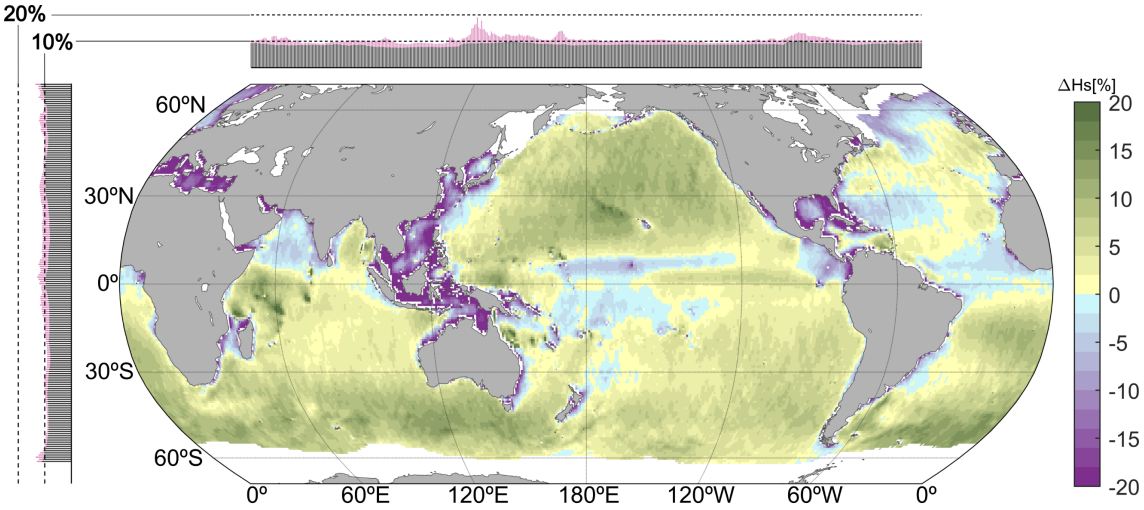


Figure SM1: Global ensemble bias assessment. Mean bias relative to satellite altimetry observations in mean H_s. The panels above and beside the map show the 25th (dark gray) and 75th (pink) percentiles of the inter-model standard deviation as a function of longitude (horizontal panel) and latitude (vertical panel). The number of ensemble members used in the calculation is indicated in **Table SM2**.

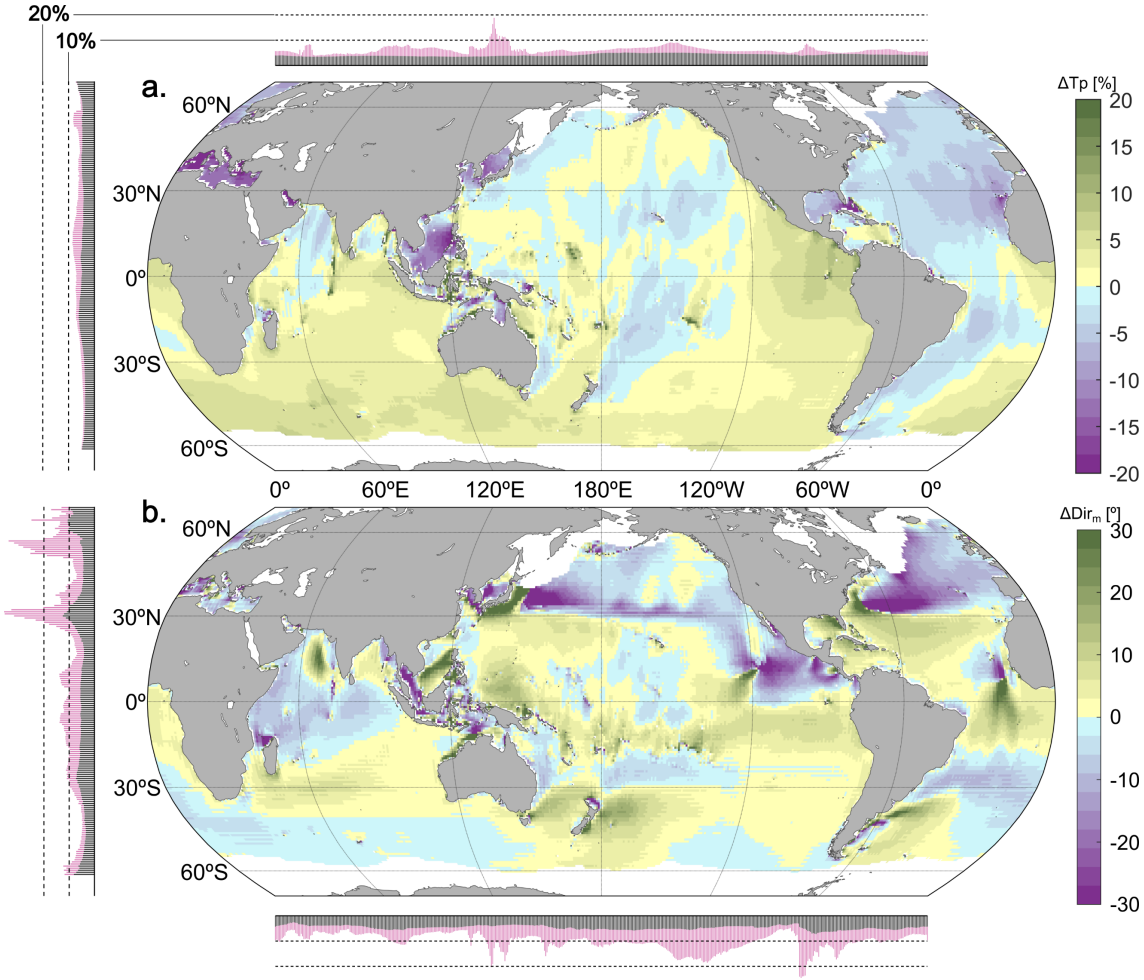


Figure SM2: Global ensemble bias assessment. Mean bias relative to ERA5 reanalysis in (a) mean T_p and (b) mean Dir_m. The panels above and beside each map show the 25th (dark gray) and 75th (pink) percentiles of the inter-model standard deviation as a function of longitude (horizontal panels) and latitude (vertical panels). The number of ensemble members used in the calculation is indicated in **Table SM2**.

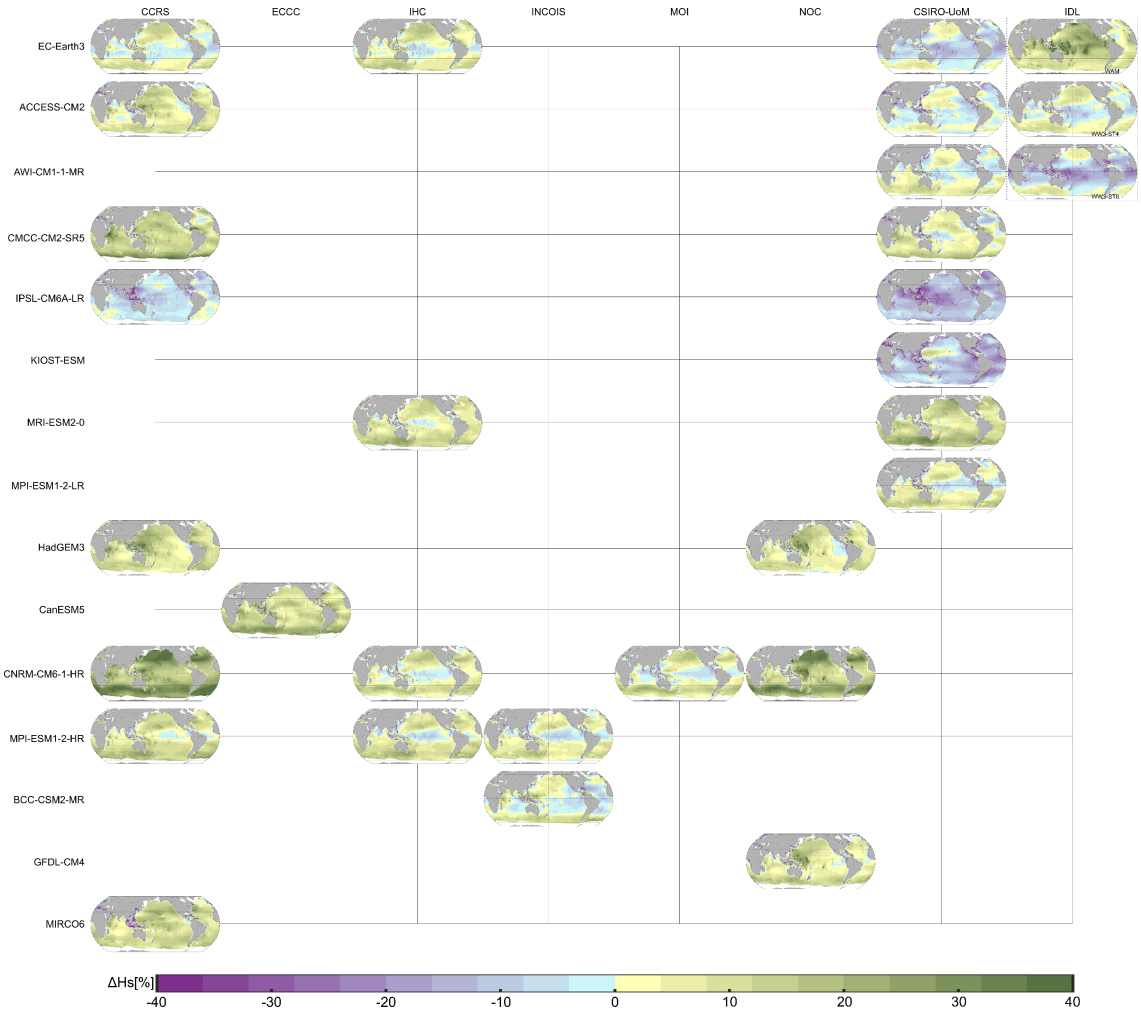


Figure SM3: Global individual-member bias assessment in mean H_s. Bias relative to ERA5 reanalysis in historical mean H_s for each ensemble member.

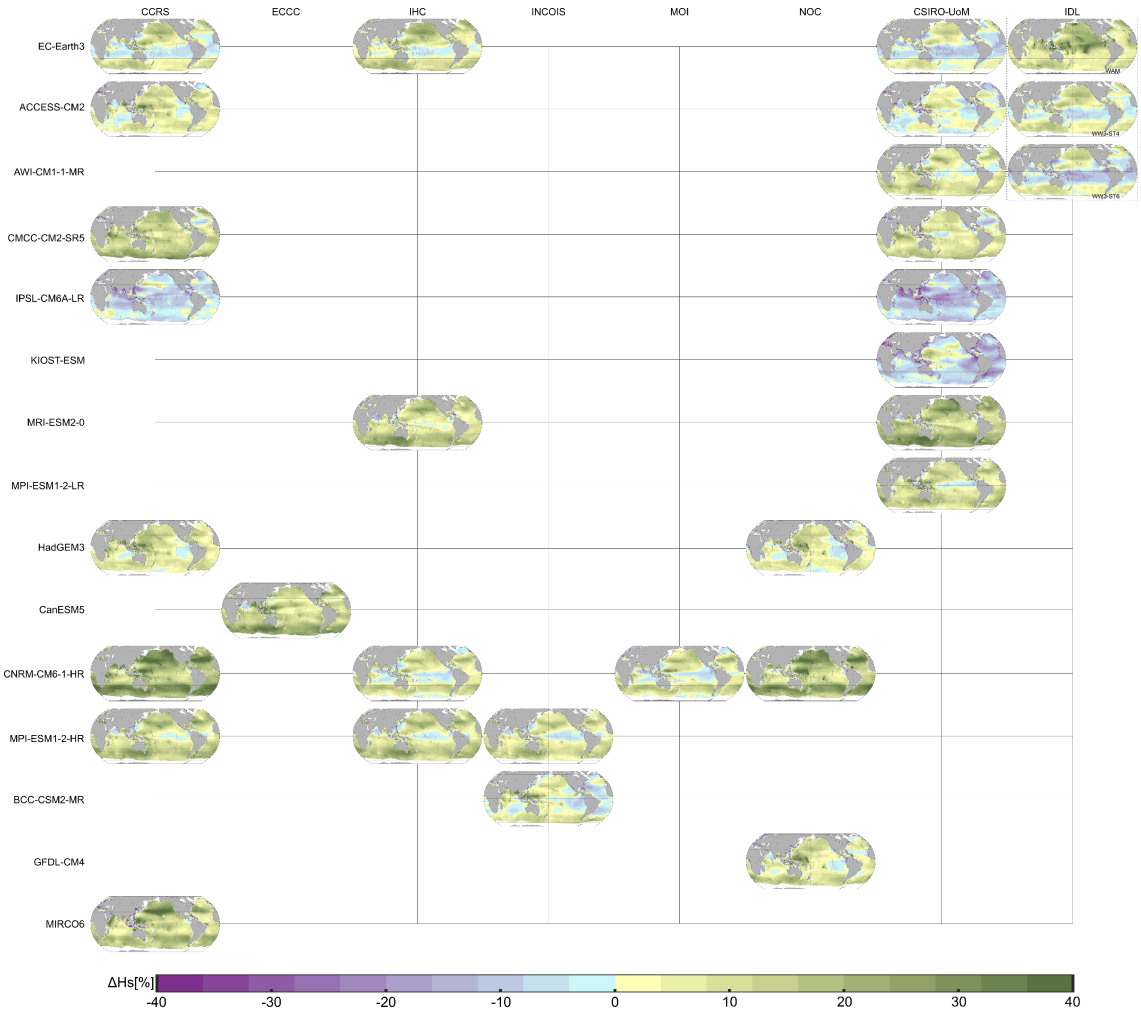


Figure SM4: Global individual-member bias assessment in 95th percentile H_s. Bias relative to ERA5 reanalysis in historical 95th percentile Hs for each ensemble member.

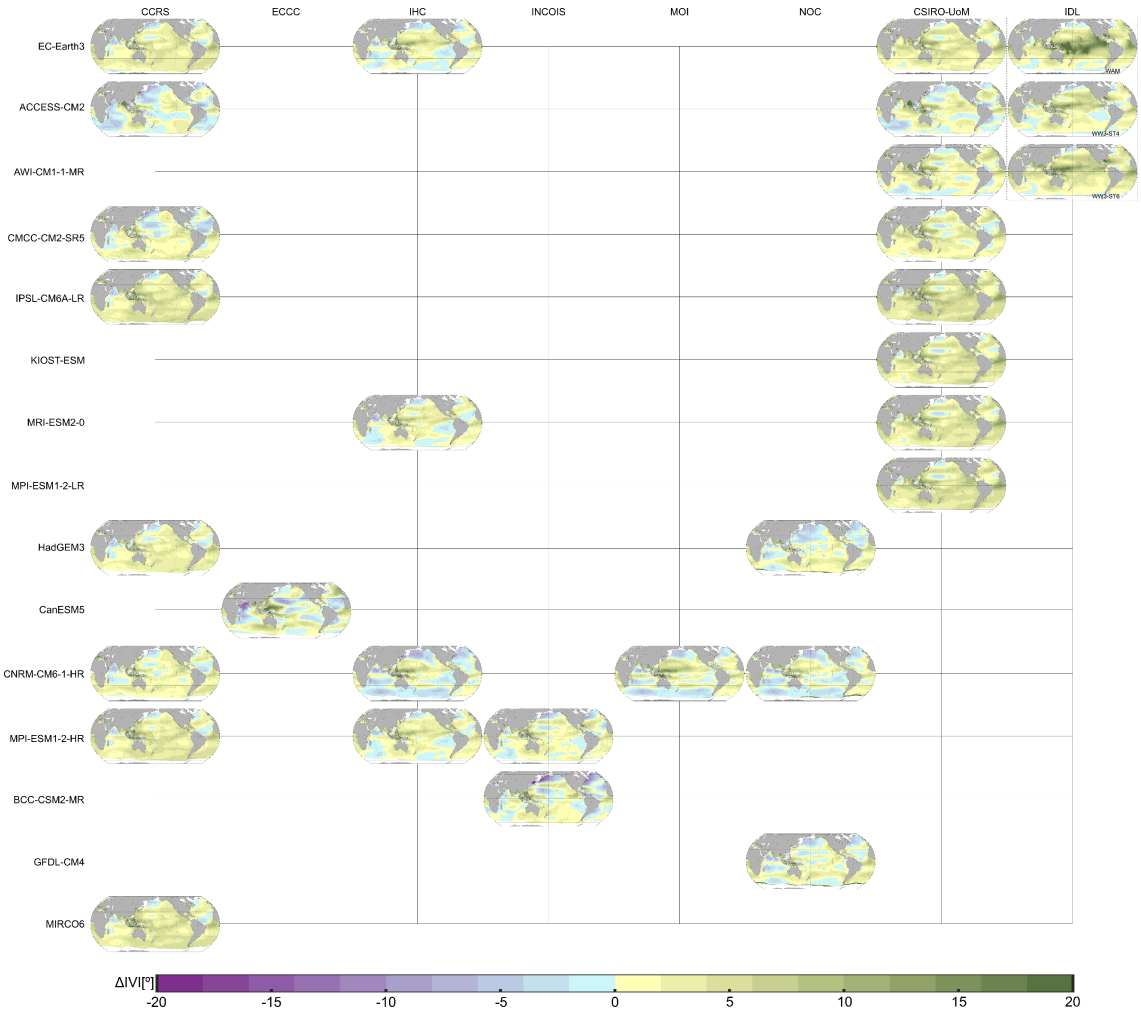


Figure SM5: Global individual-member bias assessment in monthly variability index. Bias relative to ERA5 reanalysis in historical monthly variability index (see Methods) for each ensemble member.

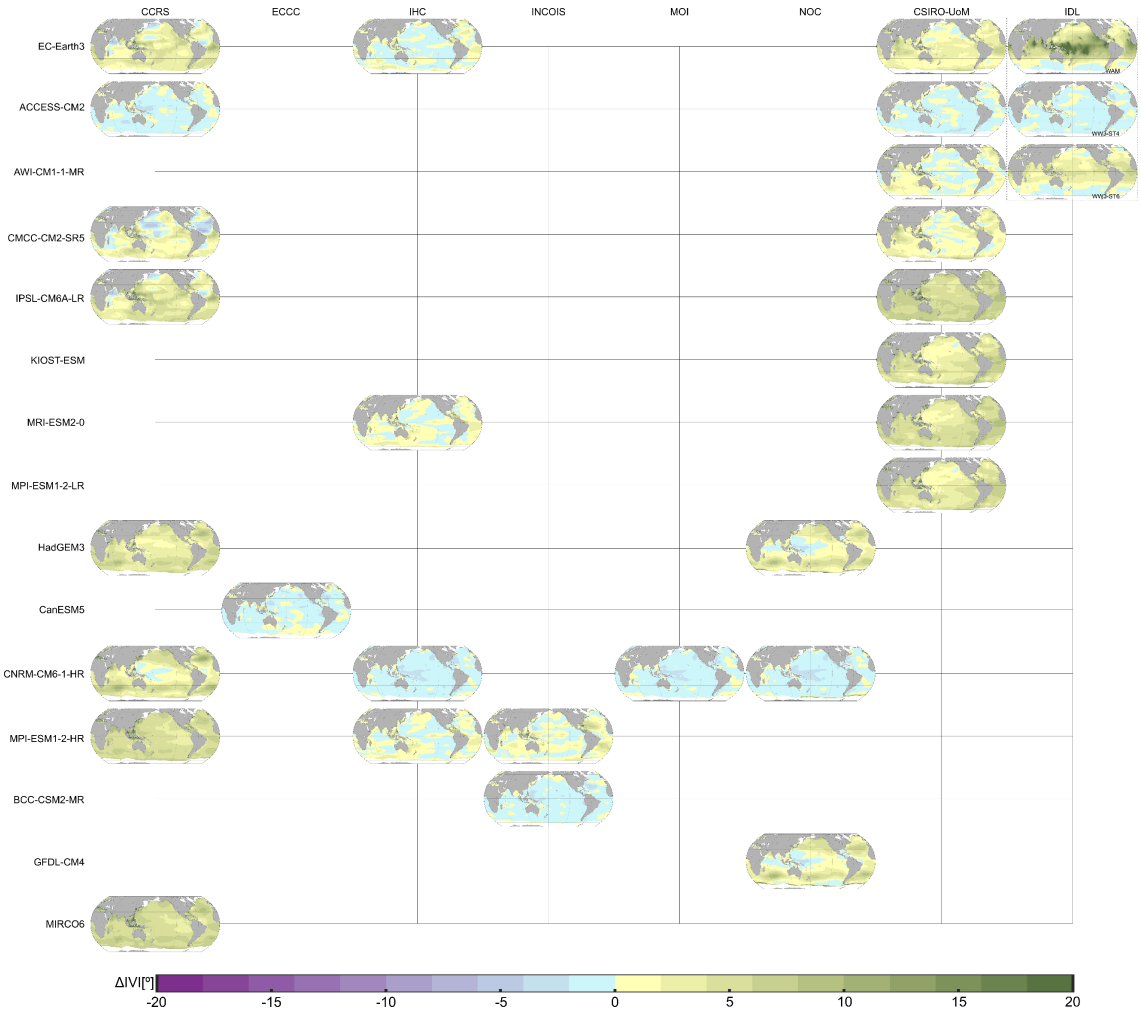


Figure SM6: Global individual-member bias assessment in interannual variability index. Bias relative to ERA5 reanalysis in historical monthly variability index (see Methods) for each ensemble member.

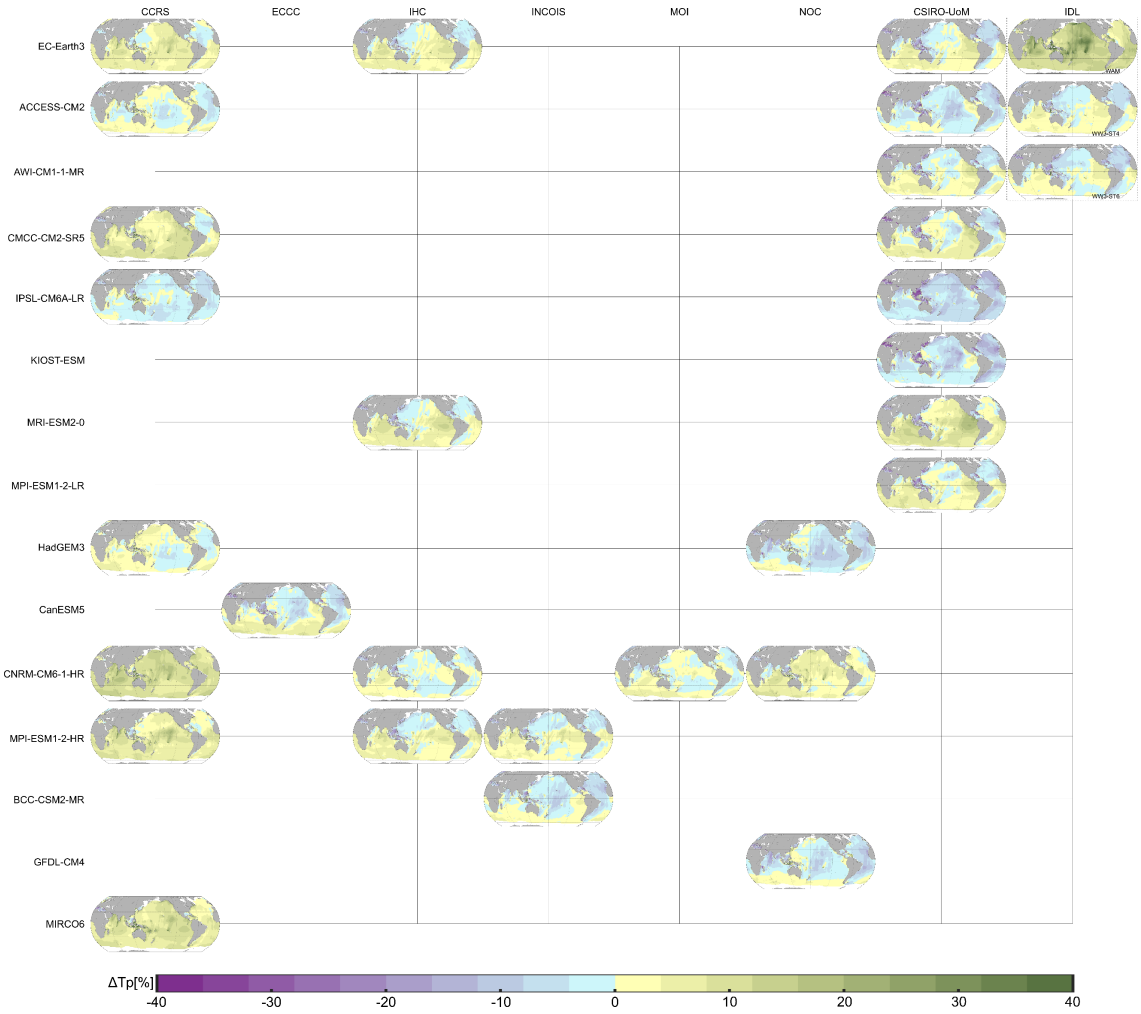


Figure SM7: Global individual-member bias assessment in mean T_p. Bias relative to ERA5 reanalysis in historical mean T_p for each ensemble member.



Figure SM8: Global individual-member bias assessment in mean Dir_m. Bias relative to ERA5 reanalysis in historical mean Dir_m for each ensemble member.

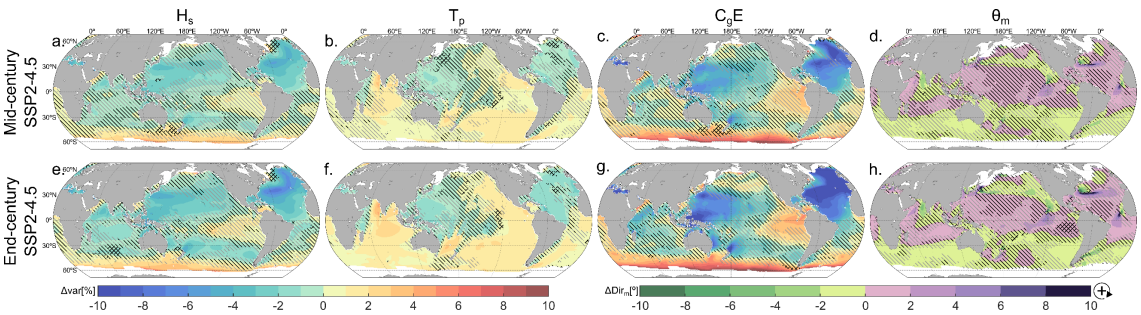


Figure SM9: Projected changes in mean wave climatologies. Projected changes in (a, e) H_s, (b, f) T_p, (c, g) C_gE, and (d, h) Dir_m. Changes are shown for the SSP2–4.5 scenario. Projected changes in scalar variables are expressed as relative changes for mid-century (2036–2065; a-d) and end-century (2071–2100; e-h) relative to the reference period (1985–2014). Projected changes in Dir_m are expressed as absolute changes (degrees) for the same time horizons. *Robust change* is shown without hatching; *conflicting change* with black cross-hatching; *emerging but not fully robust change* with gray diagonal hatching; and *non-robust change* with black diagonal hatching (see Methods for a full description of the uncertainty representation). The number of ensemble members used in the calculation is indicated in **Table SM2**.

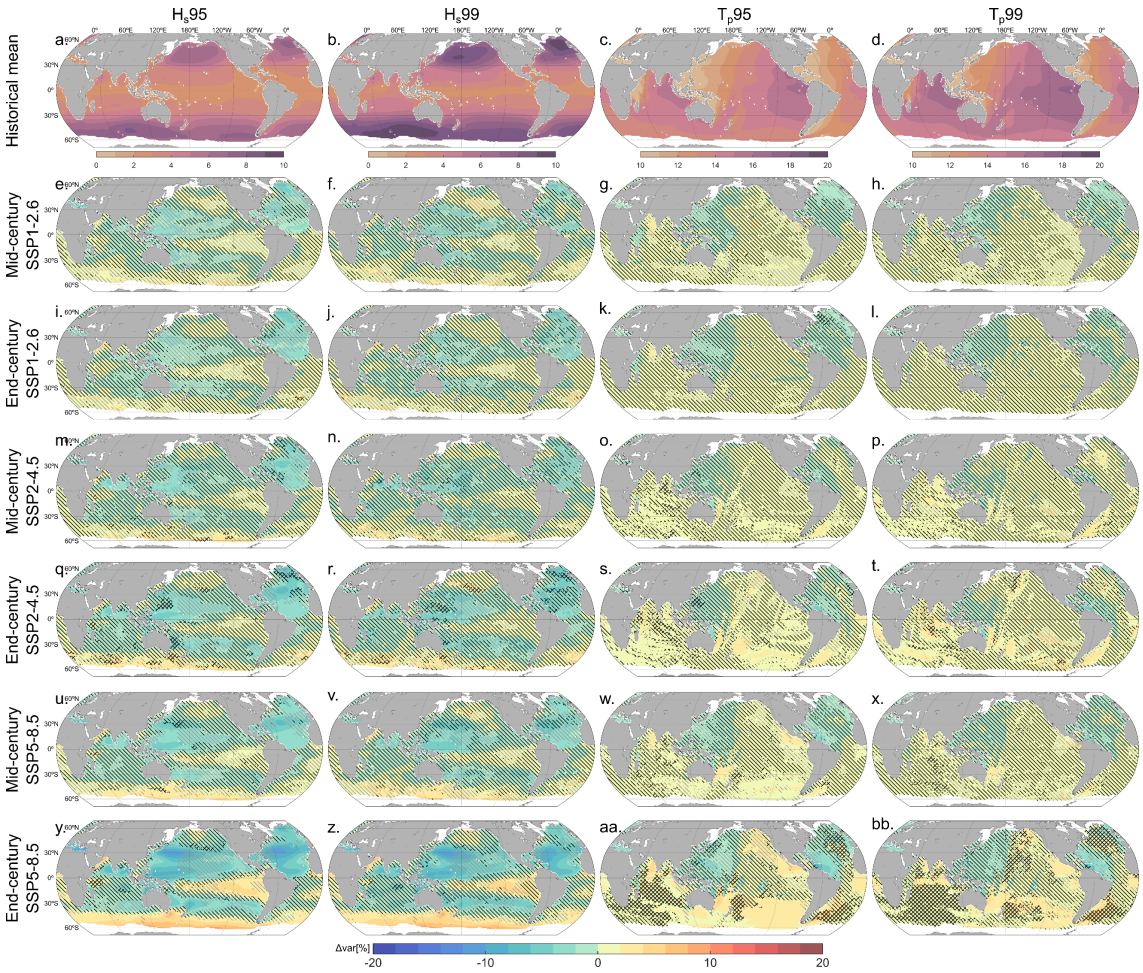


Figure SM10: Projected changes in percentile wave climatologies. Historical ensemble mean of (a) 95th percentile H_s, (b) 99th percentile H_s, (c) 95th percentile T_p and (d) 99th percentile T_p. Projected changes in (column: 1) 95th percentile H_s, (column: 2) 99th percentile H_s, (column: 3) 95th percentile T_p and (column: 4) 99th percentile T_p. Changes are shown for the SSP1–2.6 (rows: 2-3), SSP2–4.5 (rows: 4-5) and SSP5–8.5 (rows: 6-7) scenarios. Projected changes in scalar variables are expressed as relative changes for mid-century (2036–2065; rows: 2, 4, 6) and end-century (2071–2100; rows: 3, 5, 7) relative to the reference period (1985–2014). *Robust change* is shown without hatching; *conflicting change* with black cross-hatching; *emerging but not fully robust change* with gray diagonal hatching; and *non-robust change* with black diagonal hatching (see Methods for a full description of the uncertainty representation). The number of ensemble members used in the calculation is indicated in **Table SM2**.

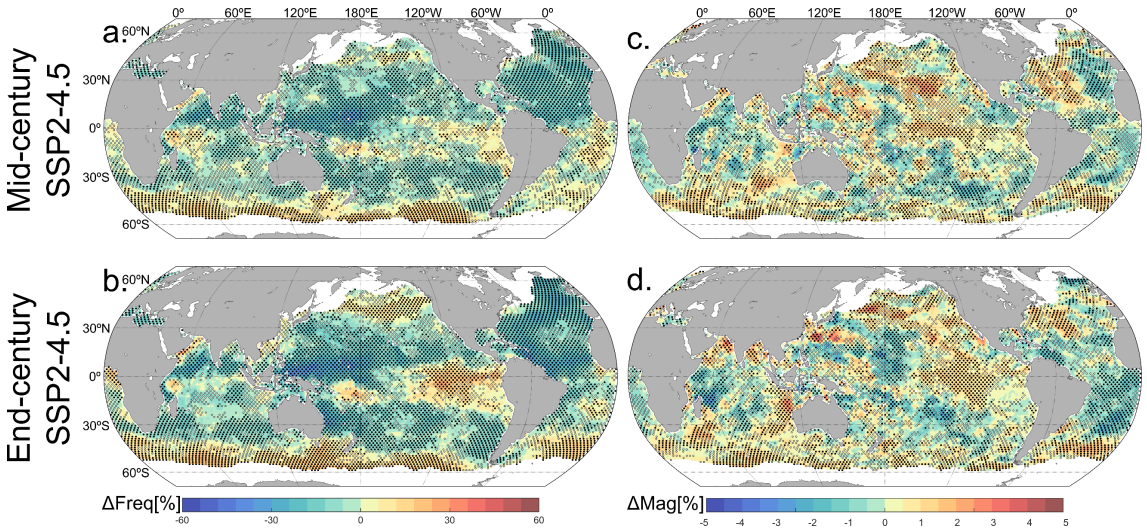


Figure SM11: Projected changes in threshold exceedances. Projected changes in (a-b) frequency of occurrence and (c-d) magnitude. Changes are shown for the SSP2–4.5 scenario. Projected changes are expressed as relative changes for mid-century (2036–2065; a, c) and end-century (2071–2100; b, d) relative to the reference period (1985–2014). *High-agreement change* is shown with filled black stippling; *moderate-agreement change* with empty black stippling; and *low-agreement change* without overlay (see Methods for a full description of the uncertainty representation). The number of ensemble members used in the calculation is indicated in **Table SM2**.

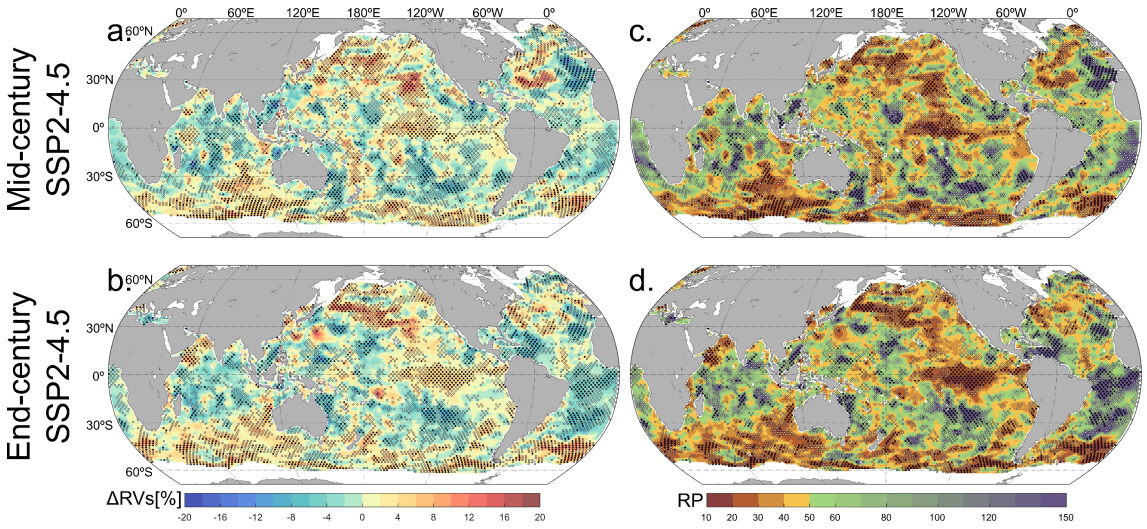


Figure SM12: Projected changes in in return levels and return periods. (a-b) Projected changes in the 50-year return values of H_s and (c–d) projected return periods of the historical 50-year return value of H_s. Results are shown for the SSP2–4.5 scenario. Projected changes are expressed as relative changes for mid-century (2036–2065; a, c) and end-century (2071–2100; b, d) relative to the reference period (1985–2014). Future return periods are shown for the same scenarios and time horizons (in years). *High-agreement change* is shown with filled black stippling; *moderate-agreement change* with empty black stippling; and *low-agreement change* without overlay (see Methods for a full description of the uncertainty representation). The number of ensemble members used in the calculation is indicated in **Table SM2**.

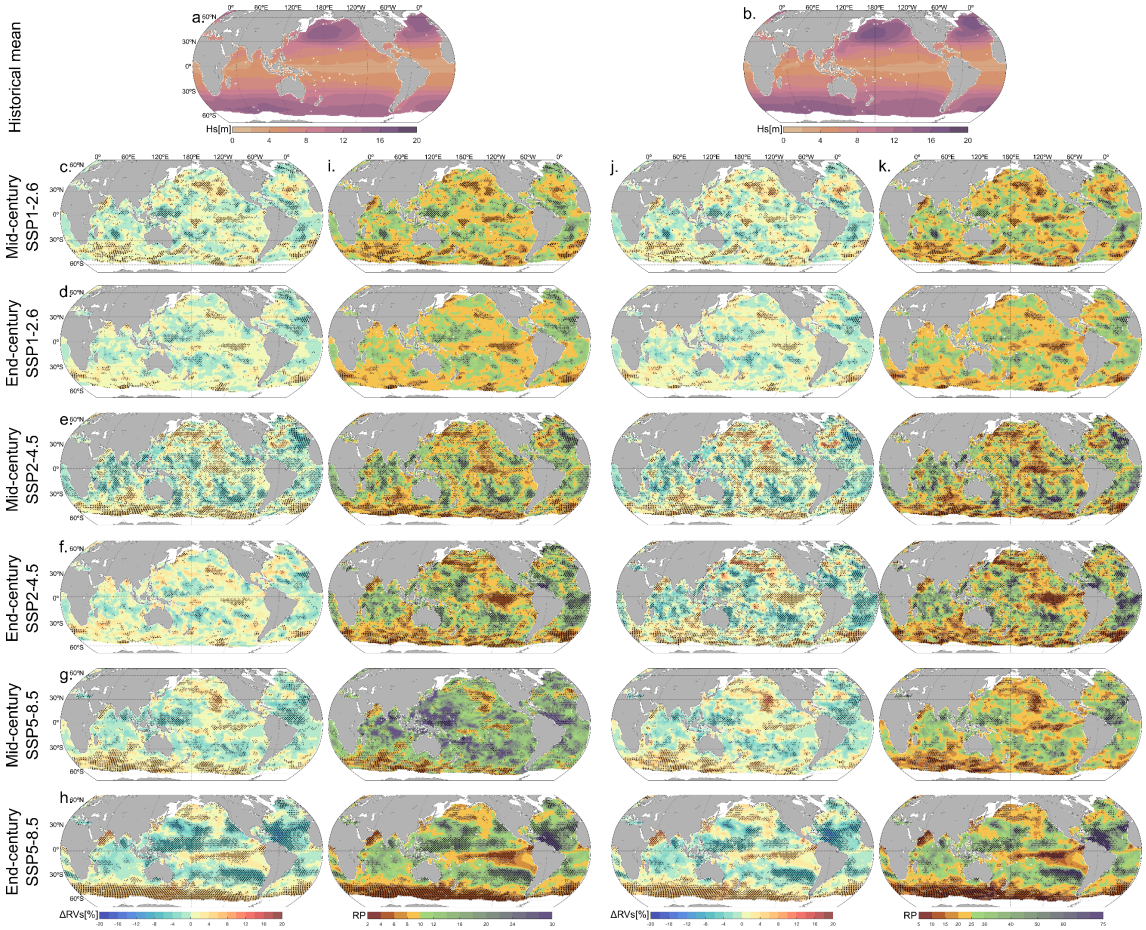


Figure SM13: Projected changes in in return levels and return periods. Historical ensemble mean (a) 10-year return values of H_s and (b) 25-year return values of H_s. (column: c) Projected changes in the 10-year return values of H_s and (column: i) projected return periods of the present-day 10-year return value of H_s. (column: j) Projected changes in the 25-year return values of H_s and (column: k) projected return periods of the historical 25-year return value of H_s. Results are shown for the SSP1–2.6 (rows: c-d), SSP2–4.5 (rows: e-f) and SSP5–8.5 (rows: g-h) scenarios. Projected changes are expressed as relative changes for mid-century (2036–2065; rows: c, e, g) and end-century (2071–2100; rows: d, f, h) relative to the reference period (1985–2014). Future return periods are shown for the same scenarios and time horizons (in years). *High-agreement change* is shown with filled black stippling; *moderate-agreement change* with empty black stippling; and *low-agreement change* without overlay (see Methods for a full description of the uncertainty representation). The number of ensemble members used in the calculation is indicated in **Table SM2**.

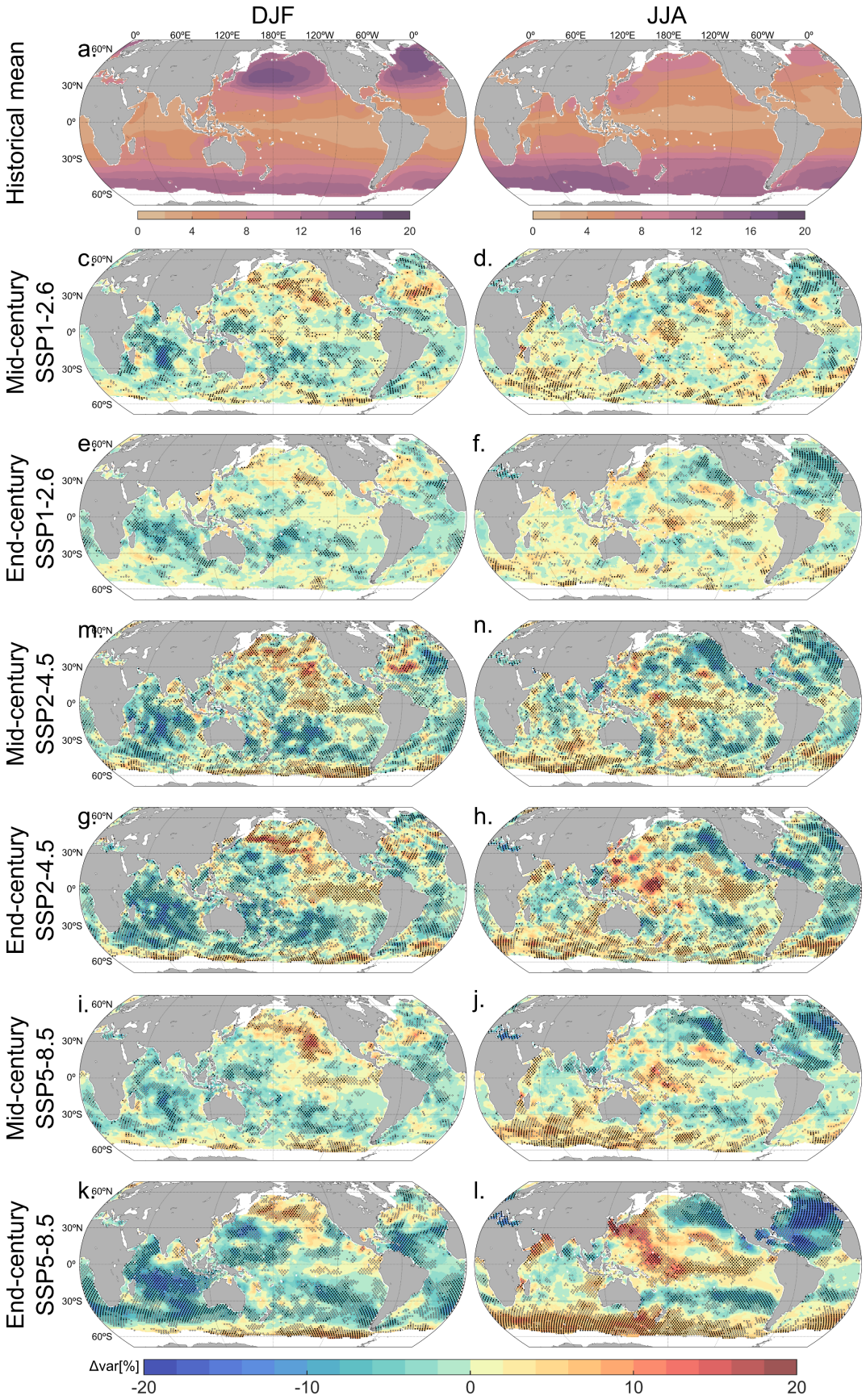


Figure SM14: Projected changes in seasonal return levels. Historical ensemble mean (a) DJF 50-year return levels of Hs and (b) JJA 50-year return levels of Hs. Results are shown for the SSP1–2.6 (panel c-e), SSP2–4.5 (panels m-h) and SSP5–8.5 (panels i-l) scenarios. Projected changes are expressed as relative changes for mid-century (2036–2065) and end-century (2071–2100) relative to the reference period (1985–2014). *High-agreement* change is shown with filled black stippling; *moderate-agreement* change with empty

black stippling; and *low-agreement* change without overlay (see Methods for a full description of the uncertainty representation). The number of ensemble members used in the calculation is indicated in **Table SM2**.

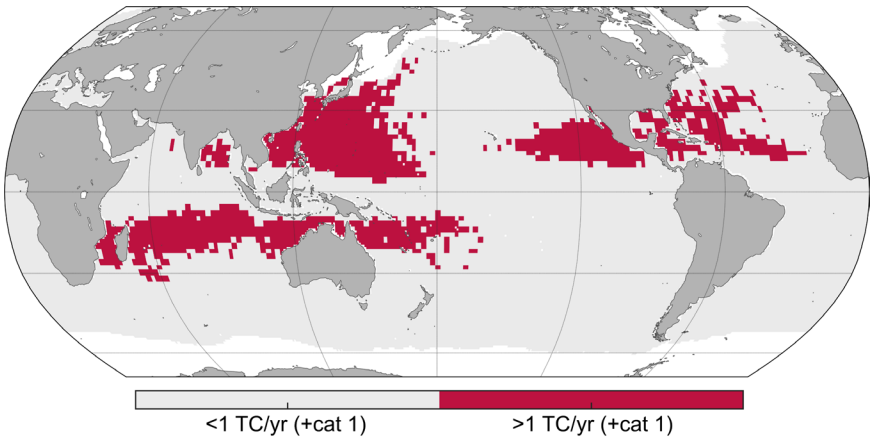


Figure SM15: Regions affected by tropical cyclones. Areas shown in red indicate regions with an annual frequency exceeding one tropical cyclone of Category 1 or higher, whereas gray denotes regions below this threshold. Tropical cyclone occurrence was derived from the International Best Track Archive for Climate Stewardship (IBTrACS) database.

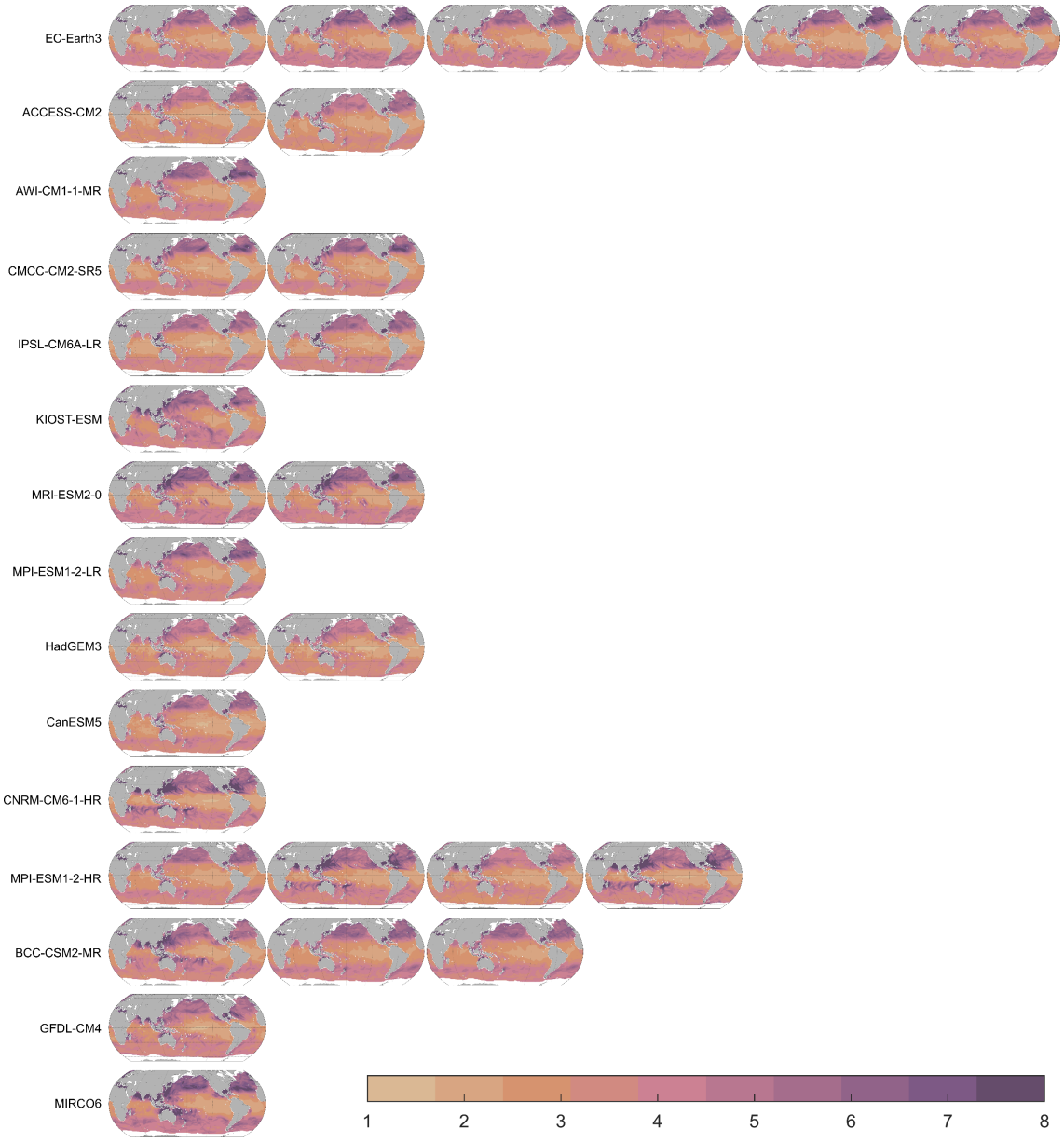


Figure SM16: Tracks of extreme events. Relationship between maximum H_s and the median H_s during the historical reference period for each ensemble member.

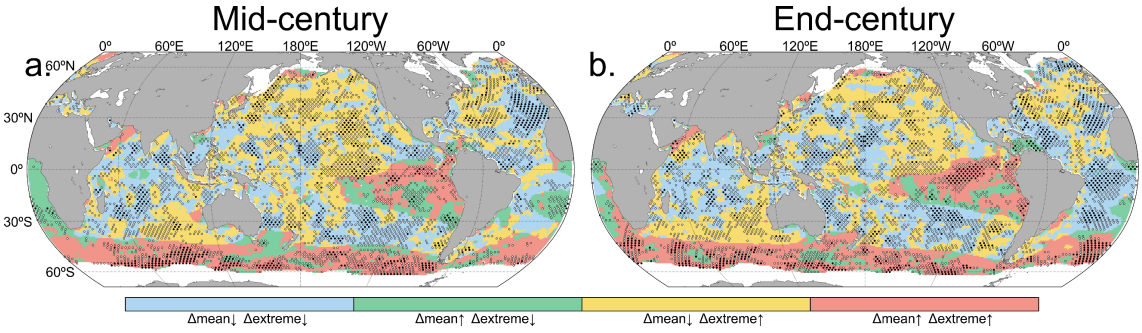


Figure SM17: Combined signals in mean versus extreme wave conditions. Projected changes in mean conditions are based on changes in mean H_s. Projected changes in extreme conditions are based on changes in the 50-year return value of H_s. Colors indicate the different combinations of the signs of change for mean and extreme conditions. Changes are assessed for the SSP2–4.5 scenario, for mid-century (2036–2065; a) and end-century (2071–2100; b) relative to the reference period (1985–2014). *High-agreement* change is shown with filled black stippling; *moderate-agreement* change with empty black stippling; and *low-agreement* change without overlay (see Methods for a full description of the uncertainty representation).

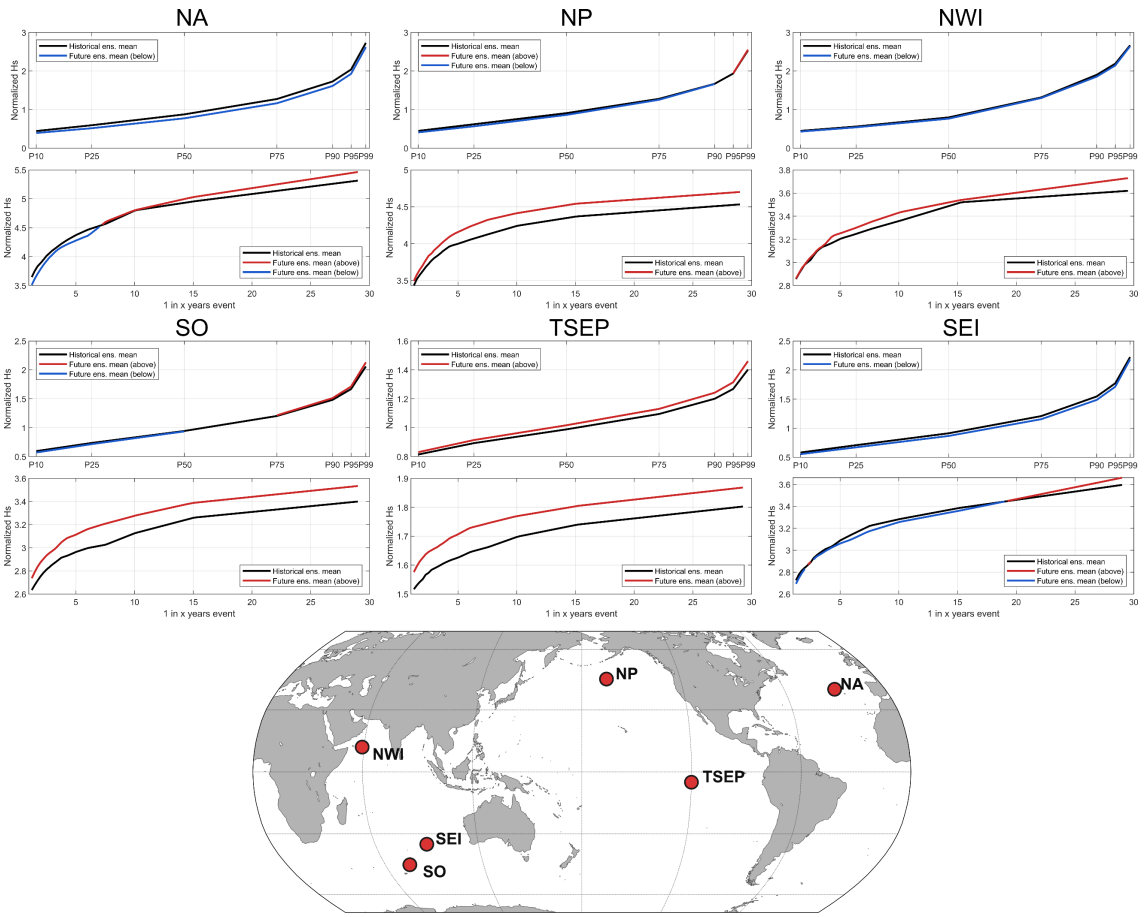


Figure SM18: Distribution of significant wave height. Distribution of H_s at target locations for the historical period and for the end-of-century period under the SSP5–8.5 scenario.

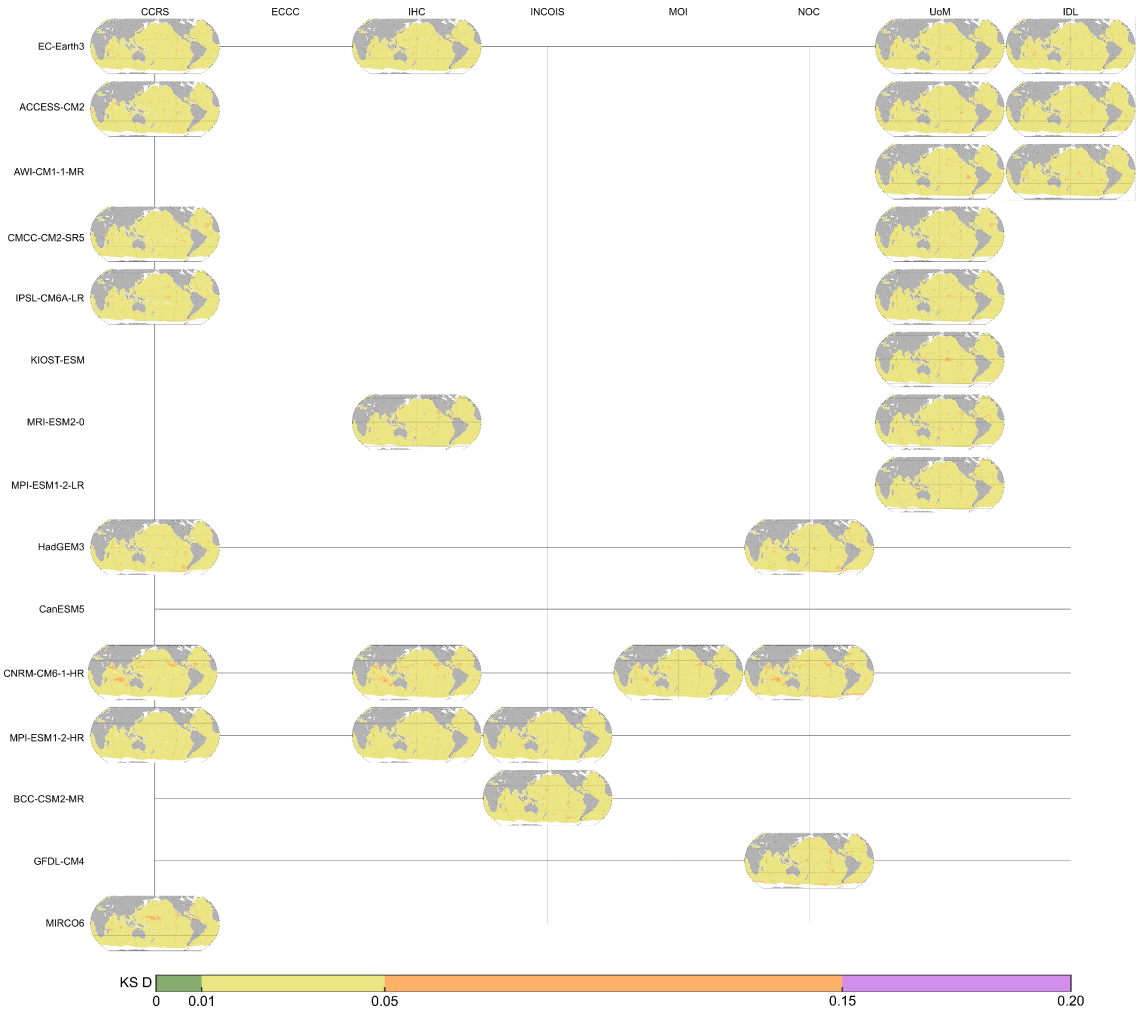


Figure SM19: Goodness-of-fit of non-stationary GEV model. Spatial distribution of the Kolmogorov-Smirnov distance (KS D) computed from probability-integral-transform (PIT) values of the historical non-stationary GEV fits (see Methods). Lower values indicate closer agreement between the fitted conditional distributions and the observed monthly maxima.